CIRP Annals - Manufacturing Technology 72 (2023) 177–180

Contents lists available at ScienceDirect

CIRP Annals - Manufacturing Technology

journal homepage: https://www.editorialmanager.com/CIRP/default.aspx

Flexible single-step fabrication of programmable 3D nanostructures by pulse-modulated local anodic oxidation

Xichun Luo*, Jian Gao, Wenkun Xie, Rashed Md. Murad Hasan, Yi Qin

Centre for Precision Manufacturing, DMEM, University of Strathclyde, Glasgow, UK

Submitted by Prof. W.B. Rowe, UK

ARTICLE INFO

Article history:
Available online 24 May 2023

Keywords:
Nano manufacturing
Process control
Pulse-modulated local anodic oxidation

ABSTRACT

A flexible single-step nanofabrication approach was developed using programmable pulse modulation local anodic oxidation for the efficient generation of various 3D nanostructures. The dependence of oxidation growth on pulse parameters was derived from parametric studies, from which an analytical process model was developed for the first time to link the pulse parameters with the geometry of 3D nanostructure with precision. The nanofabrication approach was implemented on an atomic force microscope. Experimental results show that this approach can effectively create 3D nanostructures with minimum feature sizes of sub-10 nm (lateral) and sub-nm (vertical) with nm and sub-nm level precision, respectively.

1. Introduction

Next-generation nano/quantum products/devices, such as heat-assisted magnetic recording hard disks, atomic clocks, photonic integrated circuits and plasmonic solar cells, are key enablers of future data storage, quantum computing and communication, clean energy and property growth. They are designed to have various functional nanostructures of diverse shapes on different materials. However, the lack of a low-cost flexible 'lab-to-fab' nanofabrication process to create the first prototype is a significant hurdle in these products reaching the market. Current semiconductor-based nanofabrication approaches such as optical lithography, e-beam/ion-beam lithography, self-assembly, nanoimprint lithography and scanning probe lithography, are either expensive, slow, or suffer from high defect rates due to multi-step processing for complex nanostructures. Additionally, they are also inflexible in generating various nanostructures as one type of tool (mask/stamp) can only make one type of structure [1–3].

To address these challenges, the paper proposes a new pulse-modulated local anodic oxidation (LAO) nanofabrication approach to generate various 3D nanostructures in a single step. Compared with conventional 3D nanofabrication techniques, this approach relies solely on programmable pulse modulation to achieve geometric control of 3D nanostructures in a localised anodic oxidation process. This is because a 3D nanostructure can be assumed as an assembly of many oxide nanodots, and the position, width, and height of each oxide nanodot can be correlated with the period, amplitude and width of each pulse. Therefore, various 3D nanostructures can be flexibly achieved simply through digitally programming pulse parameters in a programmable functional generator without complex operations or control systems [2].

The achievable precision of this pulse-modulated LAO nanofabrication approach relies on an in-depth understanding of the influence of the pulse processing parameters on geometries of the oxide nanodots. However, there is a large knowledge gap in the literature regarding this. As a result, the development of an accurate process model has become a significant technological challenge to further develop and implement this proposed flexible and mask-free 3D nanofabrication approach to achieve the atomic-scale precision required by the next generation of nano/quantum products/devices [1,4]. In this context, this paper first studies the dependencies of oxide growth on pulse parameters and then researches and develops a process model based on parametric effects, which are further evaluated by 3D nanofabrication experiments using an atomic force microscope (AFM). The new nanofabrication approach exploits the simplicity of pulse programming to enable single-step processing of 3D nanostructures, thus improving the quality of nanostructures by minimizing processing errors.

2. Methodology

2.1. Reaction mechanism

Fig. 1 shows a schematic of the proposed pulse-modulated LAO approach for the flexible, one-step nanofabrication of 3D nanostructures implemented on an AFM platform for simplification of demonstration. To induce oxidation, modulated pulses were introduced onto the AFM, with the tip at a negative bias to the sample substrate.

During the nanofabrication process, tip-sample bias induces a series of physical and chemical reactions. First, the bias induces the formation of a nanoscale water meniscus between the tip and the sample at a certain humidity. Then, the electric field dissociates the water molecules within the meniscus, while also directing oxyanions towards the sample substrate surface to form an oxide. Since the

* Corresponding author.
E-mail address: xichun.luo@strath.ac.uk (X. Luo).

https://doi.org/10.1016/j.cirp.2023.04.030

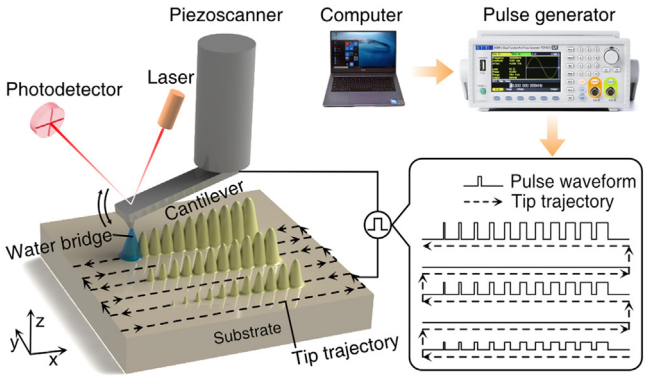

Fig. 1. Schematic of pulse-modulated local anodic oxidation.

induced amorphous oxide has a lower density than the substrate, surface protrusions are usually generated on the substrate's surface. This process of bias-induced oxidation is a Faradaic process that depends on the transport of oxyanions between the tip and sample, which is influenced by the properties of substrate material, water layer and tip-sample bias [5]. Therefore, the oxidation growth can be effectively controlled by adjusting scanning speed, humidity, charge build-up, tip-sample bias and separation [6]. Due to the high tunability and programmability of tip-sample bias, this paper focuses exclusively on the application of programmable pulse modulation to create active and accurate control of the oxidation process while keeping other process parameters constant.

2.2. Experimental setup

The experiments were performed on a Bruker Dimension 3100 AFM in ambient conditions with temperature and humidity controlled at 20 ℃ and 25%–30% RH, respectively. The sample was first cut from a p-doped silicon (100) wafer with resistivity ρ = 1–10 Ω·cm, then cleaned by sonication in an $NH_4OH/H_2O_2/H_2O$ (1:1:5) solution for 10 mins to remove surface particles and finally rinsed by deionised water and blown with a dry N_2 gas jet. AFM probes (model RTESP7) with nominal tip radius less than 10 nm, were used for the nanofabrication and imaging. In this work, the AFM was operated under raster scan mode in a scan area of 1 × 1 µm, with the x and y scanning direction as defined in Fig. 1. The enlargement of oxide due to tip scan is negligible in this work because of the use of ultra-short pulses and a slow scanning speeds at 200–3200 nm/s, where the tip displacement during the pulse width is several orders smaller than the feature size of nanodots. During the nanofabrication process, the position feedback loop of the AFM was on to control the tip-sample distance precisely during the individual oxidation and reset stages. To increase the tip-sample contact, the amplitude setpoint was set at 15% of that used in imaging [7]. The oxide patterns were imaged right after their creation and the AFM images were analysed using the NanoScope Analysis software. The modulated pulses were generated using a dual-channel arbitrary generator (TGF4042, Aim-TTi) in conjunction with an ESP-32 DevKitV1 programmed by Arduino 1.8.19 IDE software. To obtain a sufficient high electric field between the tip and the sample, the modulated pulse signal was amplified through a power amplifier (E01.A2, CoreMorrow).

3. Process model

3.1. Dependence of pulse period

As pulse period directly determines the overlapping of nanodots, this section first investigates the effect of pulse period on the generation of nanolines, which can be regarded as an ordered assembly of nanodots [8]. Herein, same amplitude of 19.6 V and width of 60 µs, but with different periods are employed.

Through the program control of function generator, pulse periods from 4 to 100 ms (corresponding to pulse duties from 1.5% to 0.06%) were applied. The oxide lines and their cross sections are shown in Fig. 2(a) and (c). It can be clearly observed that the nanoline structures with decent continuity can be produced at the pulse periods of 4–40 ms, in comparison with unoxidized surface. To compensate the dilation effect introduced by the tip radius, full width at half maximum (FWHM) is used in this work to represent the width of oxide lines. The dependence of mean oxide height and width on pulse period is shown in Fig. 2 (b). Both the height and width of oxide lines increased with the decrease of pulse period, indicating that smaller pulse periods enhance both the horizontal and vertical dimensions of the resulting nanostructures. This is because reducing the pulse period can increase the number of equal-width pulses applied in the same scan distance, resulting in the enhanced current flow during the oxidation process.

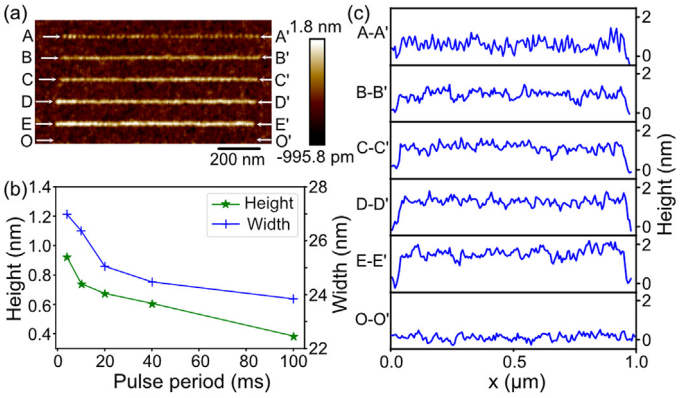

Fig. 2. (a) Schematic of nanolines created at pulse periods of 100, 40, 20, 10 and 4 ms; (b) dependence of oxide height and width on the pulse period; (c) cross-sectional profiles across each nanodot array in Fig. 2(a).

3.2. Dependence of pulse amplitude and width

To determine the effect of pulse amplitudes and widths on oxidation growth, pulses were modulated in both amplitude and width under the same period of 10 ms. Fig. 3(a) shows an array of gradient nanolines. In the x scanning direction, same amplitude pulses were used while pulse widths were varied from 15 to 300 µs, aiming to

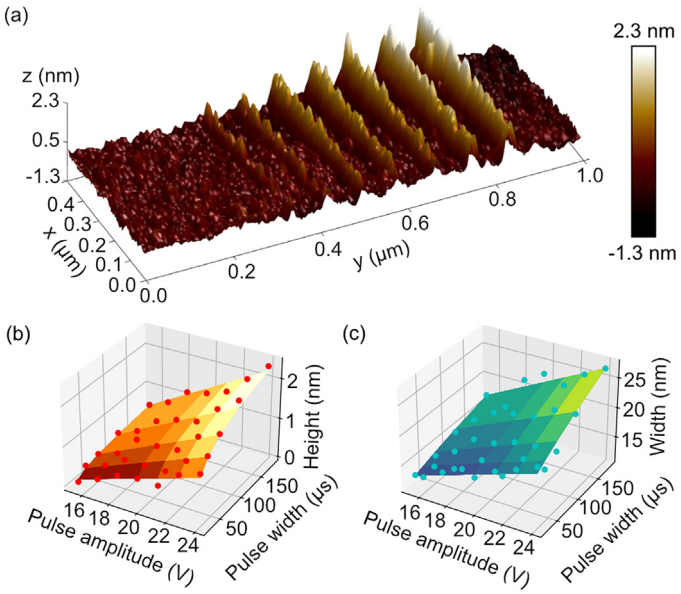

Fig. 3. (a) Schematic of a gradient nanoline array created through the modulation of pulse amplitude and width; scatter and fitting surface plots of the oxide (b) height and (c) width as functions of pulse amplitude and width.

create gradient nanolines. In the y scanning direction, the pulses were programmed to have the same width but with different amplitudes, ranging from 15.6 to 24 V.

The mean height and width of the nanolines were obtained by measuring the average of 5-equal distances taken from each nanoline. Fig. 3 (b) and (c) show their dependence on pulse amplitude and width. It can be seen that the oxide size increases linearly with pulse amplitude but logarithmically with pulse width. The dependencies can be described as:

$$h(V,t) = h_0(V) + h_1(V)\ln(t) \tag{1}$$

and

$$w(V,t) = w_0(V) + w_1(V)\ln(t) \tag{2}$$

where $h(V,t)$ and $w(V,t)$ are the oxide line height and width as a function of pulse amplitude and width when the pulse period is held constant. On the basis of these results, we can deduce that the modulation of pulse width and amplitude is a feasible way to adjust oxidation growth.

3.3. Analytical process model

The above results suggest that the relationship between oxide feature size and pulse parameters can be described by a function, which are correlated to the pulse amplitude, width and period. Therefore, if each oxide dot forming a 3D nanostructure is modelled as a Gaussian surface, its profile p can be described as:

$$p(x,y,V,t,T) = h(V,t,T)exp\left\{-\frac{(x-x_c)^2+(y-y_c)^2}{0.36[w(V,t,T)]^2}\right\} \tag{3}$$

where $h(V,t,T)$ and $w(V,t,T)$ are the oxide height and width, and V, t and T are the pulse amplitude, width and period. (x_c, y_c) is the centre coordinate of the oxide dot. Then, an arbitrary nanostructure can be regarded as an assembly of nanodots with centres at a series of 2D coordinates. The profile P for a 3D nanostructure with $N+1$ nanodots can be described as:

$$P(x,y,\boldsymbol{V},\boldsymbol{t},\boldsymbol{T}) = max\left[p_0(x,y,V_0,t_0,T_0), p_1(x,y,V_1,t_1,T_1), ..., p_N(x,y,V_N,t_N,T_N)\right] \tag{4}$$

where $\boldsymbol{V}, \boldsymbol{t}$ and $\boldsymbol{T}$ represent the amplitudes, widths and periods of a series of pulses. The centre coordinate (x_{ci}, y_{ci}) of each oxide dot can be determined through the sum of the preceding pulse periods and tip scan parameters. The oxide dot position for AFM tip operated under the raster scanning mode can be expressed as:

$$x_{ci}\left(\sum_{j=0}^{i} T_j\right) = 2Lf\left(\sum_{j=0}^{i} T_j \bmod f^{-1}\right) \tag{5}$$

and

$$y_{ci}\left(\sum_{j=0}^{i} T_j\right) = d\,\lfloor f\sum_{j=0}^{i} T_j \rfloor \tag{6}$$

where x and y are along and perpendicular to the tip scanning directions respectively as shown in Fig. 1; f, L and d are the scan rate, scan size and spacing between the adjacent scan lines, which can be set through AFM interface. If T_i follows $(n-1)f^{-1} \le T_i \le (n-0.5)f^{-1}$ (n is a positive integer), oxide dots can be created when tip is in the same scanning direction. In combination of the above equations, dot-based 3D nanostructures with profile P can be tuned through the modulation of pulse amplitude V, width t and period T. This LAO process model is based on a Faradaic process that links the oxidation growth and pulse parameters. It is therefore possible to apply this model to other combinations of substrate materials and anodic solutions where such reactions can occur, by adjusting parameters through pre-tests.

3.4. Evaluation of process model

The accuracy of the analytical process model was evaluated and verified by two sets of nanofabrication experiments. In both sets, the tip was set scanning at the speed of 200 nm/s.

A number of nanolines with different height through modulating the pulse widths were fabricated in the first set of experiment. Fig. 4 (a) shows a schematic of the modulated pulses and tip scan route. These pulses were divided into 9 groups, the time interval among them were set at 10 s through adjusting the period of the first pulse in each group. Therefore, the total period of each group of pulses equals the AFM tip scan period (10 s), allowing the creation of nanolines side-by-side. The pitch between sampling lines was set at 50 nm so that nanolines can be separated for measurement. To achieve nanolines with different heights, these pulses were kept with the same amplitude of 19.6 V, but with three different pulse widths of 20, 60 and 200 µs. Fig. 4 (b–d) show the predicted and fabricated nanolines and their feature size comparison. Good agreements were found between the predicted and fabricated line width and height. A minimum line width and height of 9.5 nm and 0.5 nm were achieved with accuracies of 1.3 nm, 0.08 nm, and precisions better than 4 nm and 0.1 nm, respectively.

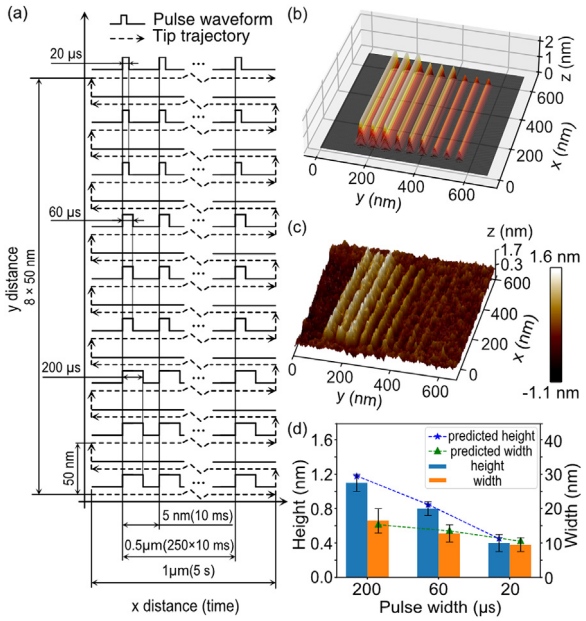

Fig. 4. (a) Schematic of modulated pulses and tip scan route, where solid lines represent the pulse waveform and dotted lines with arrows show the tip scan route; (b) process model and (c) topographical image of nanolines; (d) line widths and heights of the predicted and fabricated nanolines.

A curved surface was fabricated in the second set of experiment. Fig. 5(a) shows a schematic of the pulses applied during the tip scan, the pulse width increases linearly from 15 to 300 µs, followed by a linear decrease back to 15 µs during the second half. The pulse periods were consistently kept at 10 ms. Through applying these pulses, a 3D nanostructure was generated in just 2.5 s as shown in Fig. 5(c). A comparison with the analytically predicted 3D nanostructures (see Fig. 5(b)) reveals a good agreement. When the pulse width increases from 15 to 300 µs, the height of the fabricated nanostructure increased from 0.3 to 1.6 nm. At the same time, the width of the fabricated nanostructures varied from 7.9 to 21.2 nm and minimum width appeared to be 7.9 nm when a 15 µs pulse was applied. The results show that the proposed approach has a fabrication capability with minimum feature sizes of sub-10 nm in the lateral direction and sub-nm in height. Fig. 5(d) shows the cross-sectional profile along the gradient oxide line. The measured form error (P–P) of the fabricated nanostructures is less than 0.3 nm.

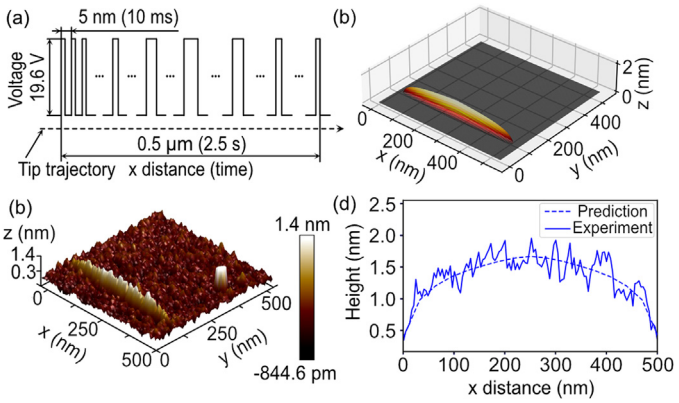

Fig. 5. (a) Schematic of modulated pulses; (b) analytical model of desired 3D curved nanostructure; (c) topographical image of resulting gradient lines; (d) comparison of cross-sectional profiles between analytical process model and measured result along the gradient line.

4. 3D fabrication

The verified analytical process model lays a solid foundation for geometrical control of fabricated 3D nanostructures. Using this model, the oxide height and width, as well as the positions of each nanodot can be precisely and effectively tuned through pulse modulation. The surface gradient can be controlled both along and perpendicular to the tip scanning directions. Therefore, 3D nanostructures can be obtained in a single scan. To further evaluate the accuracy of the proposed flexible single-step nanofabrication approach, 3D nanostructures with arbitrary shapes were fabricated. Fig. 6(a) and (b) show the predicted and fabricated 3D nanostructure with 'Nano' letter shape, which were obtained by modulating the parameters of 378 pulses. From letter 'N' to 'o', the mean heights of the fabricated results were at 1.95, 1.56, 1.22 and 0.88 nm respectively, with a deviation of less than 0.08 nm from the predicted heights of 2, 1.6, 1.2 and 0.8 nm. Additionally, a nanohemisphere and a concave lens with potential functionalisation were fabricated as shown in Fig. 6(d) and (f). Through a comparison with Fig. 6(c) and (e), good agreement was found between the analytical model and fabricated 3D nanostructures. The average form accuracy (P–P) of the measured nanostructures was 0.4 nm, with an average precision of 0.1 nm. The larger nanostructure in Fig. 6(f) was fabricated in less than 50 s when using a tip scan speed of 3.2 μm/s. The efficiency and accuracy of the proposed flexible single-step nanofabrication approach were therefore, fully demonstrated.

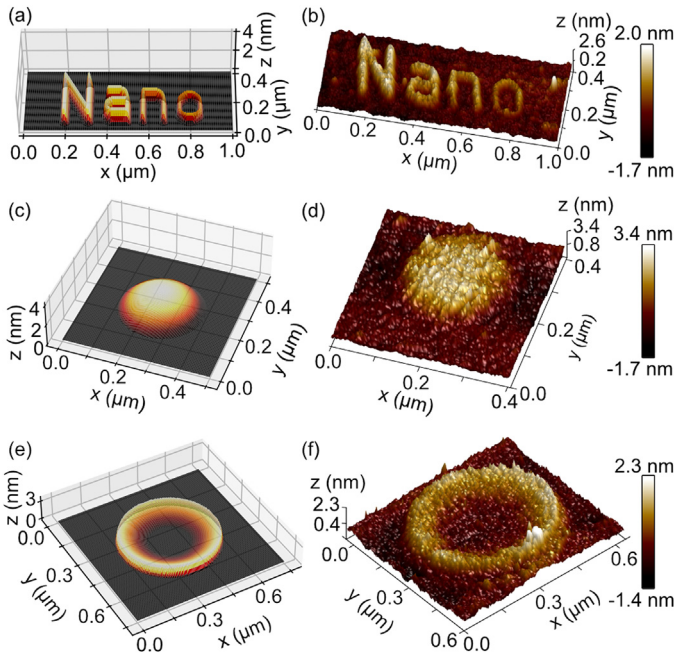

Fig. 6. Demonstration of 3D nanopatterning through pulse-modulated local anodic oxidation; (a) analytical model and (b) topographical image of 'Nano' letters; (c) analytical model and (d) topographical image of a nanohemispherical structure with a radius of 3 μm; (e) analytical model and (f) topographical image of a lens nanostructure with a radius of 10 μm.

5. Concluding remarks

This paper presented a flexible single-step pulse-modulated 3D nanofabrication approach by which various programmed nanostructures were fabricated with significantly high efficiency, flexibility and precision. Moreover, an analytical process model was proposed to establish the relationship between the pulse parameters and the desired nanostructures, which was validated by experimental tests. The high programmability of pulse parameters allows for effective, accurate and flexible control of geometries of 3D nanostructures by adjusting the pulse amplitude, width or period, without resorting to complex control systems and multi-step operations. The minimum features sizes were found to be sub-10 nm (lateral) and sub-nm (vertical) with nm and sub-nm level precision, respectively.

To make this nanofabrication approach viable industrially, tip arrays [6] or large-scale rolling nanoelectrodes [9] will have to be used so it can reach a throughput of 1 wafer/h. Assuming a tool cost of $200k and consumables cost £100k/year for 5 years of operation, the cost of ownership (CoO) of the approach will be $16/wafer, which make it very cost-competitive against current optical lithography and e-beam lithography processes with CoOs of $86/wafer and $18/wafer respectively [10,11].

Declaration of Competing Interest

The authors declare that they have no known competing financial interests or personal relationships that could have appeared to influence the work reported in this paper.

Acknowledgements

The authors would like to thank EPSRC (EP/K018345/1, EP/T024844/1, EP/V055208/1) to support this research.

References

[1] Fang F-Z, Zhang X-D, Gao W, Guo Y-B, Byrne G, Hansen H-N (2017) Nanomanufacturing—Perspective and Applications. *CIRP Annals - Manufacturing Technology* 66(2):683–705.
[2] Tseng A-A (2011) Three-Dimensional Patterning of Nanostructures Using Atomic Force Microscopes. *Journal of Vacuum Science and Technology B* 29(4):040801.
[3] Yan Y-D, Wang J-Q, Geng Y-Q, Zhang G-X (2022) Material Removal Mechanism of Multi-Layer Metal-Film Nanomilling. *CIRP Annals - Manufacturing Technology* 71 (1):61–64.
[4] Gao J, Luo X-C, Fang F-Z, Sun J-N (2021) Fundamentals of Atomic and Close-To-Atomic Scale Manufacturing: A Review. *International Journal of Extreme Manufacturing* 4(1):012001.
[5] Kuramochi H, Pérez-Murano F, Dagata JA, Yokoyama H (2003) Faradaic Current Detection During Anodic Oxidation of the H-Passivated p-Si (001) Surface with Controlled Relative Humidity. *Nanotechnology* 15(3):297.
[6] Ryu, Y.-.K., Garcia, R., 2017, Advanced Oxidation Scanning Probe Lithography Nanotechnology, 2814:142003.
[7] Graf D, Frommenwiler M, Studerus P, Ihn T, Ensslin K, Driscoll D-C, Gossard A-C (2006) Local Oxidation of Ga[Al]As Heterostructures with Modulated Tip-Sample Voltages. *Journal of Applied Physics* 99(5):053707.
[8] Calleja M, García R (2000) Nano-Oxidation of Silicon Surfaces by Noncontact Atomic-Force Microscopy: Size Dependence on Voltage and Pulse Duration. *Applied Physics Letters* 76(23):3427–3429.
[9] Hasan R-Md-M, Luo X-C, Sun J-N (2020) Rolling Nanoelectrode Lithography. *Micromachines* 11(7):656.
[10] Hazelton A-J, Wüest A, Hughes G, Litt L-C, Goodwin F (2008) Cost of Ownership for Future Lithography Technologies. *Proceedings of the SPIE* 7140:71401Q.
[11] Wieland M, Pradelles J, Landis S, Pain L, Rademaker G, Servin I, Boer G-D, Brandt P, Jager R-J-A, Steenbrink S-W-H-K (2019) Performance Validation of Mapper's FLX-1200 (Conference Presentation). *Proceedings of the SPIE* 10958:109580I.